Tissue Accumulation of Neutrophil Extracellular Traps Mediates Muscle Hyperalgesia in a Mouse Model

Kazuaki Suzuki
Department of Orthopaedic Surgery, Tohoku University Graduate School of Medicine, Japan
Masahiro Tsuchiya (tsuchiya-thk@umin.ac.jp)
Tohoku Fukushi University
Shinichiro Yoshida
Department of Orthopaedic Surgery, Tohoku University Graduate School of Medicine, Japan
Kazumi Ogawa
Tohoku University Graduate School of Biomedical Engineering
Weijian Chen
Tohoku University Graduate School of Biomedical Engineering
Makoto Kanzaki
Tohoku University Graduate School of Biomedical Engineering
Tadahisa Takahashi
Department of Orthopaedic Surgery, Tohoku University Graduate School of Medicine, Japan
Ryo Fujita
Department of Orthopaedic Surgery, Tohoku University Graduate School of Medicine, Japan
Yuqing Li
Tohoku University Graduate School of Biomedical Engineering
Yutaka Yabe
Department of Orthopaedic Surgery, Tohoku University Graduate School of Medicine, Japan
Toshimi Aizawa
Department of Orthopaedic Surgery, Tohoku University Graduate School of Medicine, Japan
Yoshihiro Hagiwara
Department of Orthopaedic Surgery, Tohoku University Graduate School of Medicine, Japan

---

Research Article

Keywords: neutrophil extracellular trap, uric acid, muscle pain, citrullinated histone H3, multiphoton microscopy imaging

Posted Date: July 23rd, 2021

DOI: https://doi.org/10.21203/rs.3.rs-576628/v2

Version of Record: A version of this preprint was published at Scientific Reports on March 9th, 2022. See the published version at https://doi.org/10.1038/s41598-022-07916-8.

Tissue accumulation of neutrophil extracellular traps mediates muscle hyperalgesia in a mouse model

Kazuaki Suzuki[1,2], Masahiro Tsuchiya[3*], Shinichiro Yoshida[1], Kazumi Ogawa[1,2], Weijian Chen[2], Makoto Kanzaki[2], Tadahisa Takahashi[1,2], Ryo Fujita[1,2], Yuqing Li[1,2], Yutaka Yabe[1], Toshimi Aizawa[1], and Yoshihiro Hagiwara[1]

[1] Department of Orthopaedic Surgery, Graduate School of Medicine, Tohoku University, Sendai, Japan

[2] Graduate School of Biomedical Engineering, Tohoku University, Sendai, Japan

[3] Department of Nursing, Tohoku Fukushi University, Sendai, Miyagi, Japan

[*] ***Corresponding author***

Masahiro Tsuchiya, DDS., PhD.

Department of Nursing, Tohoku Fukushi University

6-149-1 Kunimi-ga-oka, Sendai 981-3201, Japan

Tel: +81-22-728-6049, Fax: +81-22-233-3113

E-mail: tsuchiya-thk@umin.ac.jp

Abstract

Accumulation of uric acid (UA) during muscular trauma is a causative factor involved in the development of muscle hyperalgesia. Neutrophil extracellular traps (NETs), DNA-based reticular structures to capture UA, play a central role in the pain onset of gout attacks; however, the involvement of NETs via the elevation of local UA level in muscle hyperalgesia due to overuse injuries remains unknown. The triceps surae muscles (TSMs) in the unilateral hindlimb of mice were electrically stimulated to induce excessive muscle contraction. Mechanical withdrawal thresholds, tissue UA levels, neutrophil recruitment, protein amount of citrullinated histone 3 (citH3), a major marker of NETs, were investigated. Furthermore, whether neutrophil depletion, extracellular DNA cleavage, and administration of the urate-lowering agent febuxostat could improve muscle hyperalgesia due to NET formation was examined. CitH3 expression upon neutrophil recruitment significantly increased in the stimulated TSMs with an increase in tissue UA levels, whereas febuxostat administration improved muscle hyperalgesia with decreases in citH3 and tissue UA levels, as observed in neutrophil depletion and extracellular DNA digestion. The underlying mechanism of muscle hyperalgesia associated with locally recruited neutrophils forming NETs due to the increased tissue UA levels potentially plays a significant role in creating a vicious circle of muscle pain.

Keywords: neutrophil extracellular trap, uric acid, muscle pain, citrullinated histone H3, multiphoton microscopy imaging

Introduction

Skeletal muscle is a common source of pain that markedly impairs activities of daily living [1]. It is widely observed as a major sign of various pathologies, such as neck and shoulder pain [2], nonspecific lower back pain [3], and myofascial pain syndrome (MPS) [4]. Based on the higher lifetime prevalence of skeletal muscle pain among the labor population [5,6], muscle overuse is a key pathogenic event in developing muscle pain. Fundamentally, overuse trauma prompts muscle fibers to release extracellular adenosine triphosphate (ATP), which directly activates pain signaling through purinergic and metabotropic receptors via autocrine and paracrine functions [7 8 9 10]. Indeed, both the serum and muscle tissue levels of uric acid (UA), an end product of purine nucleotides including ATP and dead cell DNA, are reportedly increased due to the production of damaged muscle fibers [11,12 13-15].

UA has recently been recognized as a damage-associated molecular pattern (DAMP), which activates an intracellular complex called the inflammasome for processing and releasing interleukin (IL)-1β and IL-18 [16]. Our recent study using a muscle pain model by

57 the repeated electrical stimulation of the triceps surae muscles (TSMs) revealed the
58 marked recruitment of inflammatory cells, including neutrophils and macrophages,
59 producing proinflammatory cytokines, such as IL-1β and IL-18; this was due to
60 inflammasome activation, which was triggered by the increase in tissue UA levels [11 15 17].
61 Furthermore, based on the improvement of muscle hyperalgesia by the administration of
62 xanthine oxidase inhibitors, we suggested that a higher tissue UA concentration could be
63 a causative factor of mechanical hyperalgesia [11]. Thus, the dysregulated innate immune
64 response with hyperuricemia has been associated with gout among various
65 autoinflammatory diseases; these autoinflammatory diseases are characterized by
66 unprovoked episodes of recurrent or continuous inflammation in the absence of high-titer
67 autoantibodies or antigen-specific lymphocytes [18 19 20].
68 A recent study has also supported that the dysregulated innate immune response of
69 neutrophils against monosodium urate (MSU) crystals in the gout flare is a part of the
70 autoinflammatory response because of the involvement of neutrophil extracellular traps
71 (NETs) [21]. The release of NETs, a unique defense mechanism continuing from cell death
72 (NETosis), is regarded as a valuable target for disease pathogenesis in gout [21 22 23]. NETs
73 are primarily composed of their own DNA released as reticular structures with an
74 oxidative burst in order to capture and eliminate pathogens, including DAMPs[22 23], and

75 citrullinated histone H3 (citH3) plays a central role in NETosis. Interestingly, NETs also
76 contribute to aggregating neutrophilic proinflammatory mediators, thereby limiting, but
77 prolonging the inflammatory status [22]. Indeed, NETs are not only a DAMP after
78 degradation, but also a potential source of UA with extracellular nucleotide metabolism
79 [23]. Thus, research findings regarding the underlying mechanism of UA accumulation with
80 a focus on NETs in damaged muscle tissues will facilitate the development of an
81 integrative therapeutic strategy for chronic muscle pain.
82 Although the involvement of NET-mediated processes in numerous painful diseases,
83 including gout and rheumatoid arthritis, has been reported [21 22], no reports have described
84 the relationship between NETs and muscle pain. Therefore, using a muscle pain model
85 with muscle overuse, we examined whether neutrophils play a key role in developing
86 muscle pain via NET production triggered by increased UA levels.
87
88 **Results**
89 **MSU stimulation induces NETs and muscle pain in the TSMs**
90 To investigate whether MSU crystals induced NETs in skeletal muscle tissues, as shown
91 in previous studies, we first performed the intramuscular injection of MSU by following
92 a method reported in our previous study (Fig. 1) [11]. Compared to those of the control

93 group, the MNTs of the MSU group significantly decreased after the intramuscular
94 injection of MSU (Fig. 1a). In terms of IHC observations, control TSMs with saline
95 injection did not show any changes, whereas the increased immunoreactivity of citH3 and
96 Gr-1 was located around the outer edge of MSU (Fig. 1b). Western blotting using the
97 TSM tissues stimulated with MSU on day 2 showed significant increases in citH3 (Fig.
98 1c) and Ly6G (Fig. 1d). Additionally, IL-1β expression in the TSMs injected with MSU
99 significantly increased on day 2 (Fig. 1e).
100
101 **Excessive muscle contraction caused by repeated EPS induced mechanical**
102 **hyperalgesia with elevated NET production in the skeletal muscle tissues**
103 We next confirmed whether excessive muscle contraction by EPSs induced NET
104 formation associated with an increase in tissue UA levels (Fig. 2). As previously shown
105 in our studies [11,17], the MNTs of the stimulated TSMs significantly decreased due to
106 repeated stimulation, compared to those of the contralateral muscle, and were
107 significantly decreased, with the minimum MNT noted on day 7 (Fig. 2a). Reduced MNTs
108 in the stimulated TSMs increased again after 7 consecutive days of electrical stimulation,
109 and MNTs between the control (non-stimulated) and MSU (stimulated) groups were not
110 significant on day 11 (Fig. 2a). The tissue samples on day 7 were mainly used in our

111 analyses based on the above results. Among the TSM samples on day 7, tissue UA levels
112 in the stimulated TSMs were significantly higher than those in the contralateral TSMs
113 (Fig. 2b).

114 IHC analysis indicated distinct distribution patterns of citH3 immunoreactivities,
115 which colocalized with Ly6G immunoreactivities in the stimulated TSMs, but not in the
116 non-stimulated TSMs (Fig. 2c). Hematoxylin and eosin staining showed typical skeletal
117 muscle tissue histology in both groups (data not shown). Further confirming these
118 observations, western blotting indicated that the relative density of citH3 (Fig. 2d) and
119 Ly6G (Fig. 2e) normalized to the loading control (total H3 and GAPDH, respectively)
120 were significantly increased in the stimulated TSMs on day 7 compared with those in the
121 non-stimulated TSMs. The time-series experiment of citH3 protein in comparison with
122 ipsilateral to contralateral TSM tissues during and after EPS is shown in Fig. 2f. The
123 protein amount ratio of citH3 showed the highest value on day 7 with repeated EPS,
124 whereas it recovered to the level on day 0 after stopping the stimulation. IL-1β mRNA
125 expression was significantly increased in the stimulated TSMs than in the non-stimulated
126 TSMs (Fig. 2g).

127

128 **DNase treatment ameliorated muscle hyperalgesia and NET induction owing to**

repeated EPS

To confirm the pathological significance of NETs in muscle hyperalgesia, we administered DNase I to degrade extracellular DNA, including NETs, and demonstrated its impact on muscle hyperalgesia (Fig. 3). Intravenous administration of DNase I significantly increased the MNT values (Fig. 3a) and decreased tissue UA levels (Fig. 3b) in the stimulated TSMs. Consistent with these observations, IHC (Fig. 3c) and western blotting analyses (Fig. 3d and e) indicated that DNase I administration decreased the citH3 expression, but not the protein concentration of Gr-1. Additionally, IL-1β mRNA expression in the stimulated TSMs decreased following DNase I administration (Fig. 3f). Importantly, DNase administration reduced not only citH3, but also tissue UA levels despite the same intensity and duration of the repeated EPS application.

Neutrophil depletion ameliorated muscle hyperalgesia and NET induction owing to repeated EPS

Given the absolute necessity of neutrophil recruitment for NET induction, we next examined the effects of an experimental neutrophil depletion by prior treatment with anti-Gr-1 antibody on muscle hyperalgesia (Fig. 4). Neutrophil depletion resulted in a significant increase of the MNT in the stimulated hindlimbs (Fig. 4a) and reduced tissue

147 UA levels (Fig. 4b) in the TSMs with repeated EPS. Similar to the IHC images showing
148 weaker immunoreactivity of citH3 and Gr-1 in the neutrophil-depleted group than in the
149 control group (Fig. 4c), neutrophil depletion significantly decreased the relative ratio of
150 citH3 (Fig. 4d) and IL-1β mRNA expression (Fig. 4e) in the stimulated TSMs compared
151 with the control mice injected with the same amount of normal rat IgG. Notably, the tissue
152 UA level in the stimulated TSMs was decreased with experimental neutrophil depletion.
153
154 **Febuxostat treatment relieved muscle hyperalgesia due to repeated EPS**
155 Since our recent study reported that the decrease in tissue UA levels resulted in the
156 improvement of muscle hyperalgesia [11], we investigated whether the administration of
157 febuxostat, a xanthine oxidase inhibitor, influenced NET induction due to repeated EPS
158 (Fig. 5). As reported in our previous study [11], febuxostat treatment increased the MNTs
159 (Fig. 5a), and reduced tissue UA levels (Fig. 5b) and IL-1β mRNA expression (Fig. 5f) in
160 the stimulated TSMs. Consistent with these observations, IHC (Fig. 5c) and western
161 blotting analyses indicated that febuxostat administration reduced citH3 expression (Fig.
162 5d), but not neutrophil recruitment (Fig. 5c and e) in the stimulated TSMs. These results
163 indicate that high tissue UA levels would play a central role in NET induction in skeletal
164 muscle tissues with hyperalgesia.

165

166 **MPM imaging with in vivo staining for NET-like structures**

167 To confirm that repeated EPS induced neutrophil recruitment with extracellular DNA
168 release in TSM tissues, MPM imaging was performed using an in vivo immunostaining
169 method [24]. As shown in Fig. 6 and Supplemental movie, repeated EPS significantly
170 increased the fluorescence of neutrophils and extracellular DNA in TSM tissues, as
171 visualized by QD655 and SYTOX, respectively. In particular, the myofascial region
172 showed significantly more fluorescence colocalizations than the TSM myofibers.

173

174 **Discussion**

175 The present study clarified the potential pathogenesis of NETs in muscle
176 hyperalgesia (exhibiting elicited nocifensive behaviors) due to a locally higher tissue UA
177 level caused by excessive muscle contraction (Fig. 2) as well as noted the observations in
178 the TSMs with MSU injection (Fig. 1). Our findings showed a potentially "vicious cycle"
179 model of muscle hyperalgesia due to a higher tissue UA level, which develops in a
180 reciprocal manner between neutrophil recruitment and NET induction (Fig. 7).

181 NETs play an essential function in immobilizing and killing pathogens, including
182 bacteria, whilst limiting inflammation, whereas inappropriate NET release has harmful

183 late effects on tissues due to the release of cytotoxic and proinflammatory mediators with
184 NET degradation [22 23]. Delayed-onset muscle soreness, a typical muscle pain experienced
185 after excessive exercise, persists for a few days [7]. Based on the increased serum NET
186 levels after acute severe exercise [25], the characteristics of NETs would not only play a
187 crucial role in prolonging and strengthening local inflammation and pain, as observed in
188 our results, but also in general muscle physiology. Additionally, recent studies have
189 focused on the implications of NETs in numerous autoinflammatory diseases, including
190 systemic lupus erythematosus, psoriasis, and gout [21 22 26]. Interestingly, our results also
191 demonstrated that febuxostat administration, as well as the experimental neutrophil
192 depletion and DNase administration, improved the local NET accumulation associated
193 with muscle hyperalgesia (Fig. 3). Febuxostat was reported to reduce not only tissue UA
194 content, but also neutrophil recruitment in damaged tissues [27]. Thus, local NET
195 accumulation in skeletal muscles damaged by repeated excessive exercise would enhance
196 inflammation and pain with a sustainable supply of proinflammatory stimuli consisting
197 of inflammatory mediators, such as IL-1β and DAMPs, including UA.

198 MSU crystallization due to hyperuricemia is a typical causative stimulus of acute
199 and painful inflammatory responses in gout attacks [20 21]. Since our previous work showed
200 that a higher UA level in skeletal muscle tissues was a potential trigger for muscle

hyperalgesia [11], we here indicated the involvement of NETs as a crucial mediator in developing muscle hyperalgesia caused by a higher UA content in skeletal muscle tissues. However, no MSU crystals were found in the skeletal muscle tissues with excessive contraction. In terms of MSU crystallization, Martillo et al. indicated that 405 μmol/L is the solubility limit of the serum UA [28]. Our results showed that the average local UA concentration (approximately 500 μmol/L) in the stimulated muscles was higher than the abovementioned value. Because Braga et al. indicated that high concentrations of soluble UA directly activate innate immunity [16], a higher tissue UA level possibly contributes to the modulation of a microenvironment with a higher risk of NET induction as neutrophil recruitment.

In terms of a vicious cycle of a higher tissue UA level leading to NET accumulation and consequent development of muscle hyperalgesia (Fig. 7), both neutrophil depletion (Fig. 4) and DNase treatment (Fig. 3) essentially resulted not only in the improvement of muscle hyperalgesia, but also in the reduction of the tissue UA levels in the damaged skeletal muscles, as well as the febuxostat treatment (Fig. 5). Based on the activation of the inflammasome pathway in macrophages by a higher UA level [11 16], the neutrophil–macrophage interactions, as the main innate immune response, definitively contribute to the deterioration of muscle hyperalgesia. Although future

studies with appropriate designs are warranted to clarify the above aspects, these findings suggest that extracellular DNA consisting of NETs with neutrophil recruitment is potentially the main source inducing a higher UA level in skeletal muscle tissues via purine metabolism and plays a role in exacerbating muscle hyperalgesia.

Furthermore, MPM imaging of NET-like structures showed that extracellular DNA fragments were mostly colocalized with neutrophils, but not in the skeletal muscle fibers. Shinoda et al. also reported no histological changes in the stimulated skeletal muscle tissues under the same experimental conditions [10]. Thus, a higher tissue UA content with skeletal muscle overloading may predominantly depend on neutrophil recruitment followed by NETosis. Furthermore, neutrophils releasing extracellular DNA were predominantly recruited more in myofascial tissues than in muscle fibers (Fig. 6). This is consistent with the multiple lines of evidence regarding the pathomechanisms underlying the development of MPS with the characteristic irritable response in myofascial tissues [15]. Future studies are warranted to clarify the mechanisms that dominantly recruit neutrophils in myofascial tissues, thus providing new insights regarding MPS therapy and management.

Conclusions

Our findings of NET dynamics clarified the underlying mechanism of muscle hyperalgesia associated with recruited neutrophils forming NETs, which potentially cause a higher UA content in skeletal muscle tissues. Thus, the regulation of local UA metabolism while focusing on NET induction would be a potential therapeutic target to relieve muscle pain.

Methods

Experimental animals

Male BALB/c mice (5–7 weeks old) were used in this study (CLEA Japan, Tokyo, Japan). The study was carried out in compliance with the ARRIVE guidelines. Further, the experimental design, care, and use of the mice were performed according to the guidelines for animal experiments at Tohoku University. Ethical approval for this study was obtained from the Animal Research Committee of Tohoku University (approval number: 2019 MdA-070). The mice were kept in standard cages maintained in an air-conditioned room at 23 °C ± 1 °C with a 12-h light–dark cycle with ad libitum access to standard food pellets and tap water, in accordance with the National Standards Relating to the Care and Management of Laboratory Animals and Relief of Pain (Notification No. 88 of the Ministry of the Environment, Japan, April 28, 2006). General anesthesia was induced in

each mouse by the intraperitoneal injection of medetomidine (0.3 mg/kg; ZENOAQ, Fukushima, Japan), midazolam (4.0 mg/kg; SANDZ, Tokyo, Japan), and butorphanol (5.0 mg/kg; Meiji Seika Pharma Co, Tokyo, Japan). Mice were sacrificed by cervical dislocation under inhalation anesthesia with isoflurane (MSD Animal Health, Kenilworth, NJ, USA).

Repeated electrical stimulation of the triceps surae muscles

Electrical pulse stimulation (EPS) was repeatedly applied to induce excessive muscle contraction of the TSMs, as previously described [10 11 17]. Two stainless electrodes (single-stranded stainless steel wire, A-M system, Sequim, WA, USA) were transcutaneously inserted into the proximal and distal ends of the TSMs on the dorsal surface of the hindlimbs under anesthesia. EPS using a STG4004 multichannel system (MCS GmbH, Reutlingen, Germany) was performed on the muscle at 10 Hz with a 10-V amplitude and a 100-μs pulse width for 30 min everyday (day 0 through day 6). The bilateral hindlimbs were immobilized with full ankle dorsiflexion using a scotch tape to stabilize the static muscle tension during EPS. Electrodes were also applied to the contralateral hindlimbs without EPS. Within 24 h after the last EPS, the TSMs were collected, immediately frozen in liquid nitrogen, and stored at -80 °C until assayed.

Assessment of mechanical nociceptive thresholds

The mechanical nociceptive threshold (MNT) was defined as the amount of pressure required to evoke pain-related reactions such as vocalization, struggling, and hindlimb withdrawal. The MNT was evaluated using the Randall–Selitto test (MK-201D Pressure Analgesy-Meter, Muromachi Kikai Co., Tokyo, Japan) [29]. The test was performed with a cone-shaped, 2.6-mm-diameter tip attached to a scale with a display. Pressure, gradually increasing at regular intervals (10 mmHg/s) with setting the cut-off value to be 300 mmHg, was applied to the lateral side of the TSMs [11]. Since circadian rhythm affects pain sensitivity, all MNT measurements were performed in the morning. To avoid bias, the MNT assessments were analyzed by an investigator who was blinded to the experimental conditions.

Local effect of monosodium urate stimulation

To confirm the local effects of MSU on NET induction, recrystallized MSU (No. 133–13432; Wako Pure Chemicals Industries, Osaka, Japan) dissolved in saline was administered to the right TSMs (MSU group), as previously described [30 31]. Saline was administered to the contralateral TSMs (control group). The solution (100 μL) of

291 recrystallized MSU (200 μg) was injected under the fascia of the lateral head of the TSMs
292 using a 27-gauge needle. MNTs were assessed on days 0, 1, 2, and 4 post-injection. The
293 TSMs were obtained, frozen in liquid nitrogen, and stored at -80 °C until assayed.
294
295 **Pharmacological experiments related to neutrophil extracellular trap formation**
296 We administered deoxyribonuclease (DNase) I (Wako Pure Chemical Industries, Ltd.,
297 Osaka, Japan; 10 mg per kg body weight [BW] per day) through intravenous injection via
298 the tail vein [32] or febuxostat (F0847, Tokyo Chemical Industry Co., Ltd., Tokyo, Japan; 5
299 mg per kg BW per day) through intraperitoneal injection [33]. The control mice were
300 injected with the same volume of the control vehicle (saline) 15 min prior to the
301 experiment.
302 To deplete neutrophils, anti-granulocyte-differentiation antigen 1 (Gr-1; a major
303 neutrophil marker) antibody (RB6-8C5, rat IgG2b) purified from the culture supernatants
304 of a hybridoma (provided by Dr. R. Coffman) was intravenously administered into the
305 mice (Gr-1 group) once every 3 days at a dose of 5 mg/kg BW [34 35], because the injection
306 effectively causes neutropenia for at least a few days [36,37]. The control mice were also
307 injected with an equivalent amount of normal rat IgG (Jackson Laboratories, Bar Harbor,
308 ME) (IgG group).

309

310 **Measurement of tissue uric acid levels**

311 The frozen muscles (30 mg) were homogenized in 300 μL of lysis buffer (30 mM Tris,
312 100 mM sodium chloride, 1 mM ethylenediaminetetraacetic acid, 1% Triton X-100, 2.5
313 mM sodium fluoride, 2 mM sodium polyphosphate, 1 mM sodium orthovanadate, 1 mM
314 phenylmethylsulphonyl fluoride, 10 μg/mL aprotinin, 1 μg/mL pepstatin, and 5 μg/mL
315 leupeptin) and then the lysate was centrifuged at 12,000 × g for 15 min at 4 °C. The
316 supernatants were collected for the assay of tissue UA levels and western blotting. The
317 tissue UA levels were measured using an assay kit (Cayman Chemical Company, Ann
318 Arbor, USA) following the manufacturer's instructions.

319

320 **Quantitative reverse transcription polymerase chain reaction**

321 Total RNA was extracted from the TSM tissues using TRIzol (Molecular Research Centre
322 Inc., Cincinnati, OH, USA). cDNA was prepared using a Transcriptor First Strand cDNA
323 Synthesis Kit (Roche, Basel, Switzerland). The primer sequences used were as follows:
324 IL-1b: F5'-TGG TGG GGG TTC TCT GTG GTT-3' and R5'-TTG AGG CGG CTT TCT
325 TTG TCC-3' and EF1a1 (internal control primer): F5'-TCG CTT TGC TGT TCG TGA
326 C-3' and R5'-TGG GGT GGC AGG TGT TAG-3'. The relative expression levels of each

mRNA were calculated as a function of EF1a1 expression, as previously described [11 17].

Immunohistochemistry

The TSM tissues were snap-frozen in liquid nitrogen and embedded in a Tissue-Tek OCT compound (Sakura Finetek, Tokyo, Japan). The cryosections were transversely cut into 5-µm thickness using a cryostat (CM1850; Leica, Nussloch, Germany) and mounted on coated glass slides, followed by acetone fixation. After washing and incubating with a blocking buffer (5% bovine serum albumin [BSA] in Tris-buffered saline with 0.1% Tween-20) including 10% normal goat serum (Nichirei Biosciences Inc., Tokyo, Japan) for 30 min. The slides were incubated with a polyclonal rabbit anti-citH3 antibody (ab5103; 10 ng/mL; Abcam, Waltham, MA, USA) and anti-Gr-1 antibody (RB6-8C5, rat IgG2b; 10 ng/mL; BioLegend, San Diego, CA, USA) in a blocking buffer for 2 h at room temperature (RT). Subsequently, the slides were incubated for 1 h with an Alexa Fluor 488-conjugated goat anti-rabbit IgG (A-11034, Life Technologies, Carlsbad, CA, USA; dilution, 1:750) for anti-citH3 and an Alexa Fluor 555-conjugated goat anti-rat IgG (A- 21434, Life Technologies; dilution, 1:750) for Gr-1 at RT. After washing, the slides were incubated with 4,6-diamidino-2-phenylindole (Sigma–Aldrich; dilution, 1:500) for nuclear staining. Images were

captured using a fluorescence microscope (Olympus FV1000; Olympus, Tokyo, Japan) equipped with an oil-immersion objective lens (UApo/340 40×/NA 1.35). The images were analyzed using Fiji/ImageJ software (NIH, Bethesda, MD, USA). At least three images from each slide were captured at 200X magnification. To avoid bias, a few animals were used for immunohistochemistry (IHC), and two slides/animals were analyzed. After confirming the reproducibility, representative images were obtained.

Immunoblotting

The lysates extracted from the TSM tissues were adjusted to 4.0 mg/mL with a lysis buffer using a BCA Protein Assay Kit (Thermo Fisher Scientific, Waltham, MA, USA). In brief, 30 μL of samples were loaded for 5%–12% SDS-polyacrylamide gel electrophoresis and transferred to Immobilon-P polyvinylidene difluoride membranes (Merck, Kenilworth, NJ, USA) [38]. The protein-transferred membranes were blocked with 5% BSA in Tris-buffered saline with 0.1% Tween-20 and then incubated at 4 °C overnight with anti-citH3 (ab5103; 2 μg/mL), anti-histone H3 (ab1791; 1 μg/mL; Abcam), anti-Ly6G (127602; 2 μg/mL; Biolegend), and anti- GAPDH (#2118; 1:1000 dilution; Cell Signaling, Beverly, MA, USA). The membranes were washed, followed by incubation at RT for 1 h with HRP-conjugated secondary antibodies (1:10,000 dilutions of #ab6734; Abcam; and

1:5,000 dilutions of #32460; Thermo Fisher Scientific). Next, a signal using a chemiluminescence reagent, was obtained from SuperSignal West Femto Maximum Sensitivity Substrate (Thermo Fisher Scientific), and the band intensity was detected using the Image Quant TL system (GE Healthcare, Chalfont St Giles, UK).

Multiphoton microscopy imaging using in vivo staining of NET-like structures

To detect NETs through in vivo staining, two types of fluorescent reagents, anti-Gr-1 antibody conjugated to Qdot655 (QD-Gr-1Ab, 3.0 μg per mouse) to detect neutrophils and SYTOX Green (Thermo Fisher Scientific, 1 μL of 5 mM solution per mouse) to detect extracellular DNA, were used [38] [39] [24], and anti-Gr-1 antibodies were prepared by conjugation to Qdot 655 using the SAIVI rapid antibody labeling kit (Invitrogen). The conjugated antibodies were purified using a size-exclusion column, and its concentration was determined by measuring the absorbance at 679 nm. After 24 h from EPS on day 7, QD-Gr-1Ab and SYTOX were intravenously injected at 20 min before animal sacrifice under anesthesia. Mice were fixed by transcardiac perfusion with 4% paraformaldehyde in PBS, and the TSM tissues were subjected to multiphoton microscopy (MPM) imaging. An upright A1R-MP multiphoton microscope (Nikon) equipped with a Ti-sapphire laser (Mai-Tai Deep See, Spectra-Physics), GaAsP non-descanned detectors, and a water-

immersion objective lens (CFP75 Apo LWD 25x/NA1.1) was used for image recording with an excitation laser consistently set at 920 nm, with an area size of 510 μm × 510 μm and a resolution of 600 dpi. The wavelengths for detection using emission filter cubes were 492/SP nm for second-harmonic generation signals (blue channel), 525 ± 50 nm for SYTOX (green channel), and 629 ± 56 nm for QD-Gr-1Ab (far-red channel). By distinguishing between the muscle and myofascial area based on the second-harmonic generation signals indicating muscle and collagenous fibers [40], we obtained the fluorescence colocalization of QD-Gr-1Ab and SYTOX to quantitatively measure the accumulation of NET-like structures in each area using ImageJ software [41]. Further, representative 3D image stacks focusing on neutrophil recruitment releasing extracellular DNA were reconstructed from the sequential images in TSM structure.

Statistical analysis

Statistical analyses were performed using SPSS (IBM, Armonk, NY, USA). Analysis of the MNT time-course data was performed using two-way analysis of variance (ANOVA), and repeated measurements were compared using Tukey's post-hoc multiple-comparison test. To compare data from more than two groups from single and multiple days, one-way and two-way ANOVA with Tukey's post-hoc multiple comparison test were used for the

analysis, respectively. Western blotting and IL-1β data between two groups were analyzed using the Wilcoxon signed-rank test. Other data between two groups were analyzed using paired t-tests. All data are expressed as the mean ± standard error. Statistical significance was set at $P < 0.05$.

References

1 Fayaz, A., Croft, P., Langford, R. M., Donaldson, L. J. & Jones, G. T. Prevalence of chronic pain in the UK: a systematic review and meta-analysis of population studies. *BMJ open* **6**, e010364, doi:10.1136/bmjopen-2015-010364 (2016).

2 Hanvold, T. N. *et al.* The effect of work-related sustained trapezius muscle activity on the development of neck and shoulder pain among young adults. *Scandinavian journal of work, environment & health* **39**, 390-400, doi:10.5271/sjweh.3357 (2013).

3 van Dieen, J. H., Selen, L. P. & Cholewicki, J. Trunk muscle activation in low-back pain patients, an analysis of the literature. *Journal of electromyography and kinesiology : official journal of the International Society of Electrophysiological Kinesiology* **13**, 333-351, doi:10.1016/s1050-6411(03)00041-5 (2003).

4 Borg-Stein, J. & Simons, D. G. Focused review: myofascial pain. *Archives of physical medicine and rehabilitation* **83**, S40-47, S48-49, doi:10.1053/apmr.2002.32155 (2002).

5 Punnett, L. & Wegman, D. H. Work-related musculoskeletal disorders: the epidemiologic evidence and the debate. *Journal of electromyography and kinesiology : official journal of the International Society of Electrophysiological Kinesiology* **14**, 13-23, doi:10.1016/j.jelekin.2003.09.015 (2004).

6 Mills, S. E. E., Nicolson, K. P. & Smith, B. H. Chronic pain: a review of its epidemiology and associated factors in population-based studies. *British journal of anaesthesia* **123**, e273-e283, doi:10.1016/j.bja.2019.03.023 (2019).

7 Mense, S. Muscle pain: mechanisms and clinical significance. *Deutsches Arzteblatt international* **105**, 214-219, doi:10.3238/artzebl.2008.0214 (2008).

8 Mastaglia, F. L. The relationship between muscle pain and fatigue.

Neuromuscular disorders : NMD **22 Suppl 3**, S178-180, doi:10.1016/j.nmd.2012.10.003 (2012).

9 Dubin, A. E. & Patapoutian, A. Nociceptors: the sensors of the pain pathway. *The Journal of clinical investigation* **120**, 3760-3772, doi:10.1172/JCI42843 (2010).

10 Shinoda, M., Ozaki, N. & Sugiura, Y. Involvement of ATP and its receptors on nociception in rat model of masseter muscle pain. *Pain* **134**, 148-157, doi:10.1016/j.pain.2007.04.006 (2008).

11 Yoshida, S. *et al.* Involvement of inflammasome activation via elevation of uric acid level in nociception in a mouse model of muscle pain. *Molecular pain* **15**, 1744806919858797, doi:10.1177/1744806919858797 (2019).

12 Retamoso, L. T. *et al.* Increased xanthine oxidase-related ROS production and TRPV1 synthesis preceding DOMS post-eccentric exercise in rats. *Life sciences* **152**, 52-59, doi:10.1016/j.lfs.2016.03.029 (2016).

13 Green, H. J. & Fraser, I. G. Differential effects of exercise intensity on serum uric acid concentration. *Med Sci Sports Exerc* **20**, 55-59, doi:10.1249/00005768-198802000-00008 (1988).

14 Kono, H., Chen, C. J., Ontiveros, F. & Rock, K. L. Uric acid promotes an acute inflammatory response to sterile cell death in mice. *The Journal of clinical investigation* **120**, 1939-1949, doi:10.1172/JCI40124 (2010).

15 Chen, R., Yin, C., Fang, J. & Liu, B. The NLRP3 inflammasome: an emerging therapeutic target for chronic pain. *Journal of neuroinflammation* **18**, 84, doi:10.1186/s12974-021-02131-0 (2021).

16 Braga, T. T. *et al.* Soluble Uric Acid Activates the NLRP3 Inflammasome. *Scientific reports* **7**, 39884, doi:10.1038/srep39884 (2017).

17 Yoshida, S. *et al.* Involvement of neutrophils and interleukin-18 in nociception in a mouse model of muscle pain. *Molecular pain* **14**, 1744806918757286, doi:10.1177/1744806918757286 (2018).

18 Kastner, D. L., Aksentijevich, I. & Goldbach-Mansky, R. Autoinflammatory disease reloaded: a clinical perspective. *Cell* **140**, 784-790, doi:10.1016/j.cell.2010.03.002 (2010).

19 Mutua, V. & Gershwin, L. J. A Review of Neutrophil Extracellular Traps (NETs) in Disease: Potential Anti-NETs Therapeutics. *Clinical reviews in allergy & immunology*, doi:10.1007/s12016-020-08804-7 (2020).

20 Punzi, L., Scanu, A., Ramonda, R. & Oliviero, F. Gout as autoinflammatory disease: new mechanisms for more appropriated treatment targets. *Autoimmunity reviews* **12**, 66-71, doi:10.1016/j.autrev.2012.07.024 (2012).

21 Bodofsky, S., Merriman, T. R., Thomas, T. J. & Schlesinger, N. Advances in our understanding of gout as an auto-inflammatory disease. *Seminars in arthritis and rheumatism* **50**, 1089-1100, doi:10.1016/j.semarthrit.2020.06.015 (2020).

22 Neubert, E. *et al.* Chromatin swelling drives neutrophil extracellular trap release. *Nature communications* **9**, 3767, doi:10.1038/s41467-018-06263-5 (2018).

23 Cicco, S., Cicco, G., Racanelli, V. & Vacca, A. Neutrophil Extracellular Traps (NETs) and Damage-Associated Molecular Patterns (DAMPs): Two Potential Targets for COVID-19 Treatment. *Mediators of inflammation* **2020**, 7527953, doi:10.1155/2020/7527953 (2020).

24 Sumagin, R., Prizant, H., Lomakina, E., Waugh, R. E. & Sarelius, I. H. LFA-1 and Mac-1 define characteristically different intralumenal crawling and emigration patterns for monocytes and neutrophils in situ. *Journal of immunology (Baltimore, Md. : 1950)* **185**, 7057-7066, doi:10.4049/jimmunol.1001638 (2010).

25 Syu, G. D., Chen, H. I. & Jen, C. J. Acute severe exercise facilitates neutrophil extracellular trap formation in sedentary but not active subjects. *Med Sci Sports Exerc* **45**, 238-244, doi:10.1249/MSS.0b013e31826df4a1 (2013).

26 Gray, R. D. *et al.* Delayed neutrophil apoptosis enhances NET formation in cystic fibrosis. *Thorax* **73**, 134-144, doi:10.1136/thoraxjnl-2017-210134 (2018).

27 Kataoka, H., Yang, K. & Rock, K. L. The xanthine oxidase inhibitor Febuxostat reduces tissue uric acid content and inhibits injury-induced inflammation in the liver and lung. *European journal of pharmacology* **746**, 174-179, doi:10.1016/j.ejphar.2014.11.013 (2015).

28 Martillo, M. A., Nazzal, L. & Crittenden, D. B. The crystallization of monosodium urate. *Current rheumatology reports* **16**, 400, doi:10.1007/s11926-013-0400-9 (2014).

29 Randall, L. O. & Selitto, J. J. A method for measurement of analgesic activity on inflamed tissue. *Archives internationales de pharmacodynamie et de therapie* **111**, 409-419 (1957).

30 Ju, T.-J., Dan, J.-M., Cho, Y.-J. & Park, S.-Y. Inhibition of Inducible Nitric Oxide Synthase Attenuates Monosodium Urate-induced Inflammation in Mice. *kjpp* **15**, 363-369, doi:10.4196/kjpp.2011.15.6.363 (2011).

31 Chen, C.-J. *et al.* MyD88-dependent IL-1 receptor signaling is essential for gouty inflammation stimulated by monosodium urate crystals. *The Journal of clinical investigation* **116**, 2262-2271, doi:10.1172/JCI28075 (2006).

32 Cagliani, J., Yang, W. L., Brenner, M. & Wang, P. Deoxyribonuclease Reduces Tissue Injury and Improves Survival After Hemorrhagic Shock. *The Journal of*

surgical research **249**, 104-113, doi:10.1016/j.jss.2019.11.036 (2020).

33 Wang, S. *et al.* Febuxostat pretreatment attenuates myocardial ischemia/reperfusion injury via mitochondrial apoptosis. *Journal of translational medicine* **13**, 209, doi:10.1186/s12967-015-0578-x (2015).

34 Chen, L., Watanabe, T., Watanabe, H. & Sendo, F. Neutrophil depletion exacerbates experimental Chagas' disease in BALB/c, but protects C57BL/6 mice through modulating the Th1/Th2 dichotomy in different directions. *European journal of immunology* **31**, 265-275, doi:10.1002/1521-4141(200101)31:1<265::Aid-immu265>3.0.Co;2-l (2001).

35 Hirano, Y. *et al.* Neutralization of osteopontin attenuates neutrophil migration in sepsis-induced acute lung injury. *Critical care (London, England)* **19**, 53, doi:10.1186/s13054-015-0782-3 (2015).

36 Conlan, J. W. & North, R. J. Neutrophils are essential for early anti-Listeria defense in the liver, but not in the spleen or peritoneal cavity, as revealed by a granulocyte-depleting monoclonal antibody. *The Journal of experimental medicine* **179**, 259-268, doi:10.1084/jem.179.1.259 (1994).

37 Rakhmilevich, A. L. Neutrophils are essential for resolution of primary and secondary infection with Listeria monocytogenes. *Journal of leukocyte biology* **57**, 827-831, doi:10.1002/jlb.57.6.827 (1995).

38 Chaweewannakorn, C. *et al.* Exercise-evoked intramuscular neutrophil-endothelial interactions support muscle performance and GLUT4 translocation: a mouse gnawing model study. *The Journal of physiology* **598**, 101-122, doi:10.1113/JP278564 (2020).

39 Masuda, S. *et al.* Measurement of NET formation in vitro and in vivo by flow cytometry. *Cytometry. Part A : the journal of the International Society for Analytical Cytology* **91**, 822-829, doi:10.1002/cyto.a.23169 (2017).

40 Chaweewannakorn, C. *et al.* Imaging of muscle activity-induced morphometric changes in fibril network of myofascia by two-photon microscopy. *Journal of anatomy* **238**, 515-526, doi:10.1111/joa.13339 (2021).

41 Tsuchiya, M. *et al.* Neutrophils Provide a Favorable IL-1-Mediated Immunometabolic Niche that Primes GLUT4 Translocation and Performance in Skeletal Muscles. *Cell reports* **23**, 2354-2364, doi:10.1016/j.celrep.2018.04.067 (2018).

Acknowledgments

The authors are grateful to Dr. Shigenori Sekiai, Dr. Chayanit Chaweewannakorn, and Ms. Natsumi Emoto at the Tohoku University Graduate School of Biomedical Engineering for their technical assistance and Dr. Hiroyuki Tada at the Tohoku University Graduate School of Dentistry for the excellent advice on the study. We also thank other doctors at the Department of Orthopaedic Surgery, Tohoku University Graduate School of Medicine, for their excellent technical advice in this study.

Authors' contributions

Conceptualization: KS, MT, SY, MK, and YH; Data curation: KS, MT, and KO; Formal analysis: KS and MT; Funding acquisition: MT, SY, MK, and YH; Investigation: KS, SY, KO, WC, TT, RF, and YL; Methodology: KS, MT, WC, MK, and YL; Project administration: MT, SY, MK, YY, and YH; Resources: KS, MT, SY, KO, WC, TT, RF, and YL; Supervision: MK, TA, and YH; Validation: TT, RF, and YL; Writing – original draft: KS, MT, SY, and YH. All authors contributed to the data analysis and work presented in this paper.

Declarations

Ethics approval and consent to participate

The experimental design, care, and use of the mice were performed according to the guidelines for animal experiments at Tohoku University. Ethical approval for this study was obtained from the Animal Research Committee of Tohoku University (approval number: 2019 MdA-070).

Consent for publication

Not applicable

Availability of data and materials

The data that support the findings of this study are available from the corresponding author, MT, upon reasonable request.

Competing interests

The authors declare that they have no competing interests.

Funding

This work was supported in part by grants from the Japan Society for the Promotion of Science (nos. 16K11580 and 19K10229 to MT).

Figure Legends

Figure 1. Induction of muscle hyperalgesia and NETs with intramuscular MSU injection. (a) Time-series experiment of MNT values in the MSU- or Saline-injected (contralateral)

572 hindlimbs. (b) Representative IHC images of TSM tissue on day 2, indicating citH3
573 (green), Gr-1 (red), and DAPI (blue). Western blotting analysis of citH3 (c) and Ly6G (d)
574 amounts in TSM tissues on day 2 after intramuscular injection of MSU or Saline. The
575 relative density is normalized based on the loading control (total histone H3: total H3 and
576 GAPDH, respectively). Scale bar = 100 μm. (e) qRT-PCR analysis was performed to
577 evaluate expression levels of IL-1β, using MSU- or saline-injected TSM tissues on day 2.
578 All data are shown as mean ± SE (n = 6 - 10) and analysed using paired t-test or two-way
579 ANOVA with Tukey's post-hoc multiple comparison test for time-series of MNT values.
580 Statistical significance is indicated with * ($p < 0.05$), ** ($p < 0.01$) and *** ($p < 0.001$),
581 respectively.
582
583 **Figure 2.** Effects of repeated electrical stimulation (EPS) to induce muscle hyperalgesia
584 and NETs. (a) Time series experiment of MNT values in the stimulated and non-
585 stimulated hindlimbs (contralateral side in the same mice). (b) The uric acid level in the
586 stimulated and non-stimulated TSM tissues on day 7. (c) Representative IHC images of
587 mouse TSM tissue with or without repeated EPS on day 7, indicating citH3 (green), Gr-
588 1 (red), and DAPI (blue). Scale bar = 100 μm. (d) citH3 and (e) Ly6G amounts in TSM
589 tissues with or without repeated EPS on day 7 by western blotting analysis. The relative

590 density is normalized based on the loading control (total histone H3: total H3 and GAPDH,
591 respectively). (f) Time series experiment of citH3 induction in stimulated TSM tissues.
592 After normalization of citH3 using the total H3, a ratio of citH3 in ipsilateral side relative
593 to contralateral side was calculated in each individual. (g) qRT-PCR analysis was
594 performed to evaluate expression levels of IL-1β, using TSM tissues of control or
595 stimulated mice on day 7. All data are shown as mean ± SE (n = 4 - 9) and analysed using
596 paired t-test for comparing the mean of two different samples or two-way ANOVA
597 followed by Tukey's post-hoc multiple comparison test for time-series experiment of
598 MNT values and for comparing more than two groups. Statistical significance is indicated
599 with * ($p < 0.05$), ** ($p < 0.01$) and *** ($p < 0.001$), respectively.
600
601 **Figure 3.** Effects of DNase treatment on NETs induction associated with muscle
602 hyperalgesia. MNT values of hindlimbs (a) and the uric acid level (b) in TSM tissues in
603 sham-stimulated control and stimulated mice injected intravenously with 10 mg/kg/day
604 of DNase I or a vehicle. (c) Representative IHC images of the stimulated TSM tissue with
605 or without DNase Ⅰ administration on day 7, indicating citH3 (green), Gr-1 (red), and
606 DAPI (blue). Scale bar = 100 μm. Western blotting analysis of citH3 (d) and Ly6G (e)
607 amounts in TSM tissues on day 7. The relative density is normalized based on the loading

608 control (total H3 and GAPDH, respectively), and further calculated as a ratio in ipsilateral
609 side relative to contralateral (unstimulated) side of the same individual. (f) qRT-PCR
610 analysis was performed to evaluate expression levels of IL-1β in TSM tissues on day 7.
611 All data are shown as mean ± SE (n = 4 - 9) and analysed using unpaired t-test for
612 comparing the mean of two different samples or two-way ANOVA followed by post-hoc
613 Tukey's test for a comparison of more than two groups. Statistical significance is
614 indicated with * ($p < 0.05$), ** ($p < 0.01$) and *** ($p < 0.001$), respectively.
615
616 **Figure 4.** Effects of neutrophil depletion on NETs induction associated with muscle
617 hyperalgesia. MNT values of hindlimbs (a) and the uric acid level (b) in TSM tissues in
618 sham-stimulated control and stimulated mice injected intravenously with 5 mg/kg BW of
619 anti-Gr-1 antibodies or control rat IgGs every 3 days. (c) Representative IHC images of
620 the stimulated TSM tissue with or without neutrophil depletion on day 7, indicating citH3
621 (green), Gr-1 (red), and DAPI (blue). Scale bar = 100 μm. (d) Western blotting analysis
622 of citH3 amounts in TSM tissues on day 7. The relative density is normalized based on
623 the loading control (total H3), and further calculated as a ratio in ipsilateral side relative
624 to contralateral (unstimulated) side of the same individual. (e) qRT-PCR analysis was
625 performed to evaluate expression levels of IL-1β in TSM tissues on day 7. All data are

shown as mean ± SE (n = 4 - 8) and analysed using unpaired t-test for comparing the mean of two different samples or two-way ANOVA followed by post-hoc Tukey's test for a comparison of more than two groups. Statistical significance is indicated with * ($p < 0.05$), ** ($p < 0.01$) and *** ($p < 0.001$), respectively.

Figure 5. Effects of febuxostat treatment on NETs induction associated with muscle hyperalgesia. MNT values of hindlimbs (a) and the uric acid level (b) in TSM tissues in sham-stimulated control and stimulated mice injected intraperitoneally with 5 mg/kg BW/day of febuxostat or a vehicle. (c) Representative IHC images of the stimulated TSM tissue with or without febuxostat treatment on day 7, indicating citH3 (green), Gr-1 (red), and DAPI (blue). Scale bar = 100 μm. (d) Western blotting analysis of citH3 amounts in TSM tissues with or without febuxostat treatment on day 7. The relative density is normalized based on the loading control (total H3), and further calculated as a ratio in ipsilateral side relative to contralateral (unstimulated) side of the same individual. (e) qRT-PCR analysis was performed to evaluate expression levels of IL-1β in TSM tissues on day 7. All data are shown as mean ± SE (n = 4 - 9) and analysed using unpaired t-test for comparing the mean of two different samples or two-way ANOVA followed by post-hoc Tukey's test for a comparison of more than two groups. Statistical significance is

644 indicated with * ($p < 0.05$), ** ($p < 0.01$) and *** ($p < 0.001$), respectively.

645

646 **Figure 6.** MPM imaging of neutrophil recruitment releasing extracellular DNA due to
647 repeated electrical stimulation (EPS) as assessed by in vivo immunostaining.
648 Representative images show fluorescence colocalization of neutrophils (indicated by
649 white arrows) labelled with QD655-conjugated anti-Gr-1 antibody (red) and extracellular
650 DNA labelled with SYTOX (green) in TSM tissues (muscle fibers and myofascia zone)
651 of sham-control or stimulated mice on day 7. Muscle and collagenous fibers are visualized
652 with second-harmonic generation (blue). The graph summarizing area quantification (%)
653 of fluorescence colocalizations within myofascia or muscle fibers of TSM tissues is
654 indicated. Data are shown as the mean ± SE (n = 3). The quantification results were
655 analysed using one-way ANOVA with Tukey's post hoc test. Scale bar = 50 μm. Both a
656 and b show significant difference to all other groups at $P < 0.05$, respectively.

657

658 **Figure 7.** A simple schema of the developing pathway of muscle hyperalgesia caused by
659 a higher tissue uric acid level in the mouse model, and the effects of inhibitors at each
660 factor.

661

Figure 1

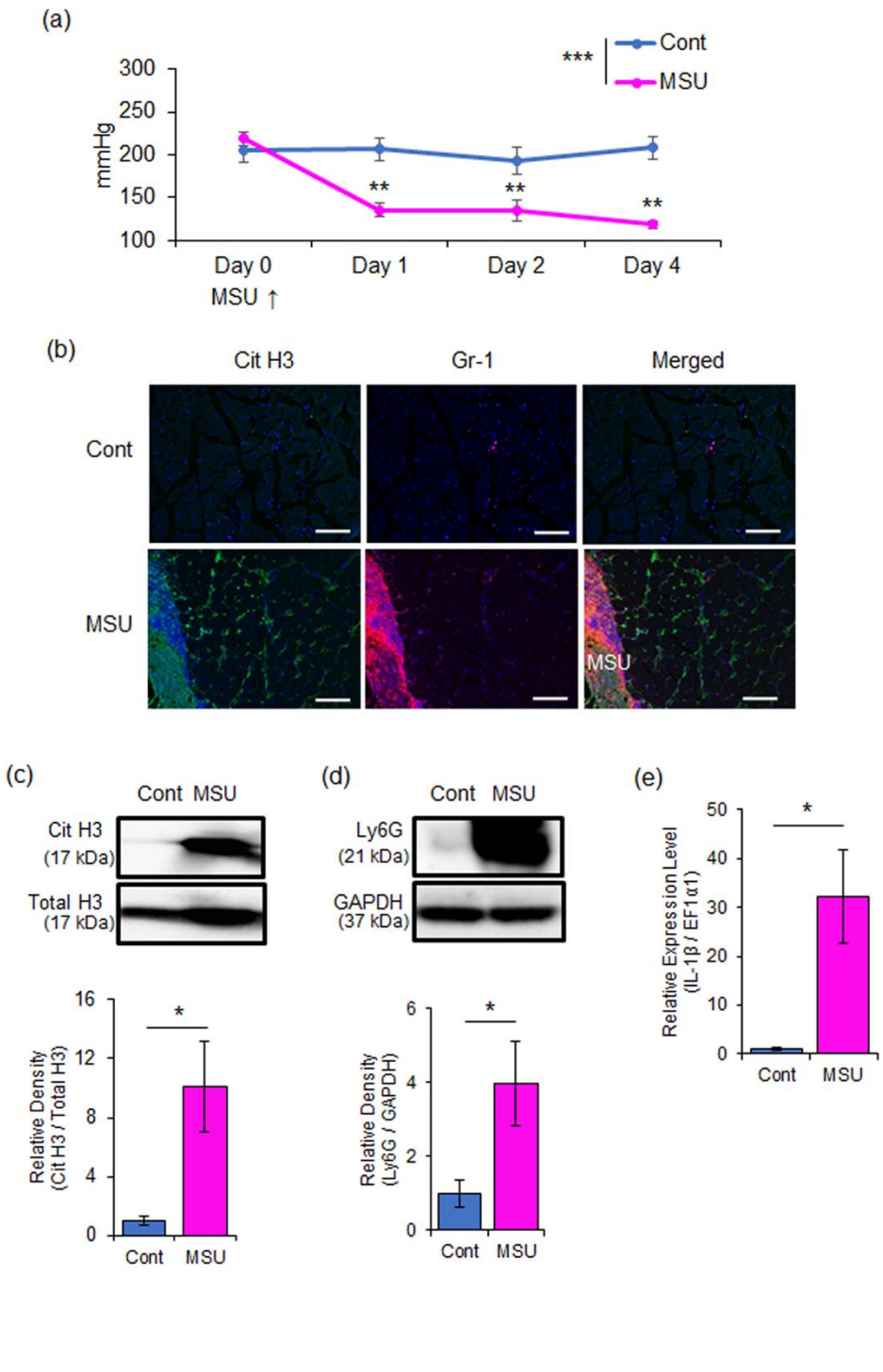
(a)
***
Cont
MSU
300
250
200
150
100
mmHg
**
**
**
Day 0
MSU ↑
Day 1
Day 2
Day 4
(b)
Cit H3
Gr-1
Merged
Cont
MSU
MSU
(c)
Cont MSU
Cit H3
(17 kDa)
Total H3
(17 kDa)
Relative Density
(Cit H3 / Total H3)
16
12
8
4
0
*
Cont
MSU
(d)
Cont MSU
Ly6G
(21 kDa)
GAPDH
(37 kDa)
Relative Density
(Ly6G / GAPDH)
6
4
2
0
*
Cont
MSU
(e)
Relative Expression Level
(IL-1β / EF1α1)
50
40
30
20
10
0
*
Cont
MSU

Figure 2

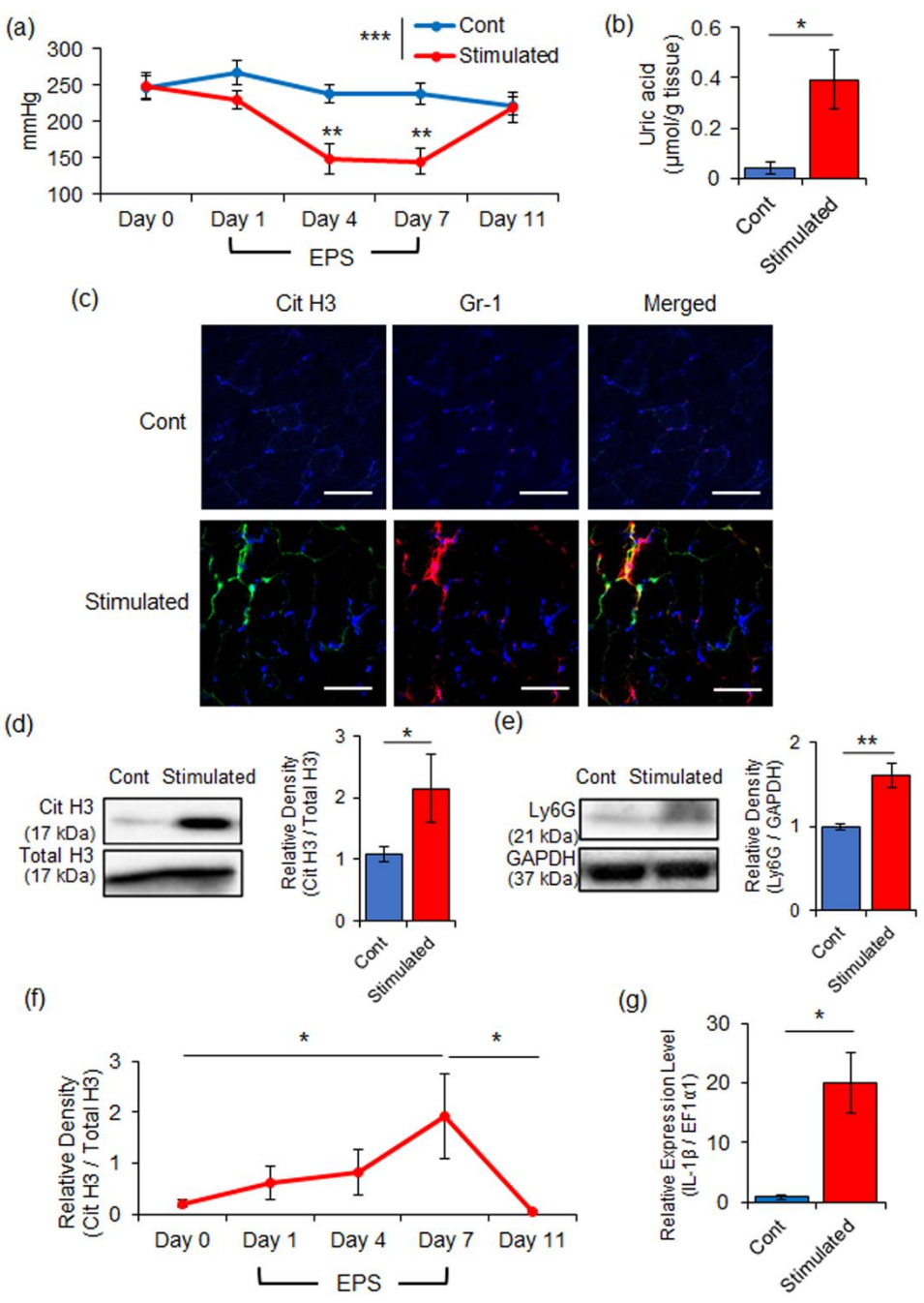
(a)
Cont
Stimulated
***
**
**
mmHg
300
250
200
150
100
Day 0
Day 1
Day 4
Day 7
Day 11
EPS
(b)
*
Uric acid
(μmol/g tissue)
0.6
0.4
0.2
0
Cont
Stimulated
(c)
Cit H3
Gr-1
Merged
Cont
Stimulated
(d)
Cont Stimulated
Cit H3
(17 kDa)
Total H3
(17 kDa)
*
Relative Density
(Cit H3 / Total H3)
3
2
1
0
Cont
Stimulated
(e)
Cont Stimulated
Ly6G
(21 kDa)
GAPDH
(37 kDa)
**
Relative Density
(Ly6G / GAPDH)
2
1
0
Cont
Stimulated
(f)
*
*
Relative Density
(Cit H3 / Total H3)
3
2
1
0
Day 0
Day 1
Day 4
Day 7
Day 11
EPS
(g)
*
Relative Expression Level
(IL-1β / EF1α1)
30
20
10
0
Cont
Stimulated

Figure 3

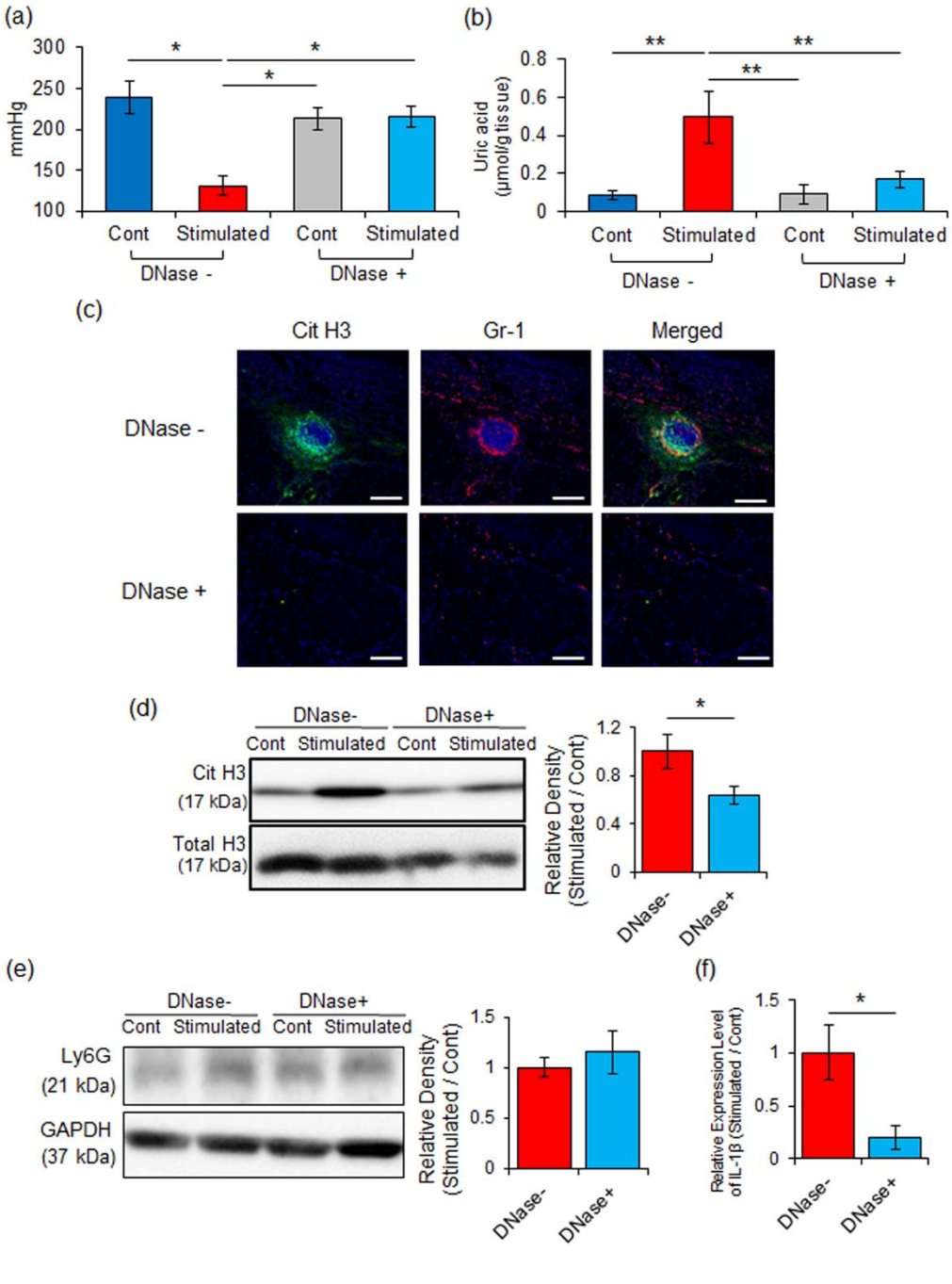
(a)
mmHg
300
250
200
150
100
*
*
*
Cont
Stimulated
Cont
Stimulated
DNase -
DNase +
(b)
Uric acid (μmol/g tissue)
0.8
0.6
0.4
0.2
0
**
**
**
Cont
Stimulated
Cont
Stimulated
DNase -
DNase +
(c)
Cit H3
Gr-1
Merged
DNase -
DNase +
(d)
DNase-
DNase+
Cont
Stimulated
Cont
Stimulated
Cit H3
(17 kDa)
Total H3
(17 kDa)
Relative Density
(Stimulated / Cont)
1.2
0.8
0.4
0
*
DNase-
DNase+
(e)
DNase-
DNase+
Cont
Stimulated
Cont
Stimulated
Ly6G
(21 kDa)
GAPDH
(37 kDa)
Relative Density
(Stimulated / Cont)
1.5
1
0.5
0
DNase-
DNase+
(f)
Relative Expression Level
of IL-1β (Stimulated / Cont)
1.5
1
0.5
0
*
DNase-
DNase+

Figure 4

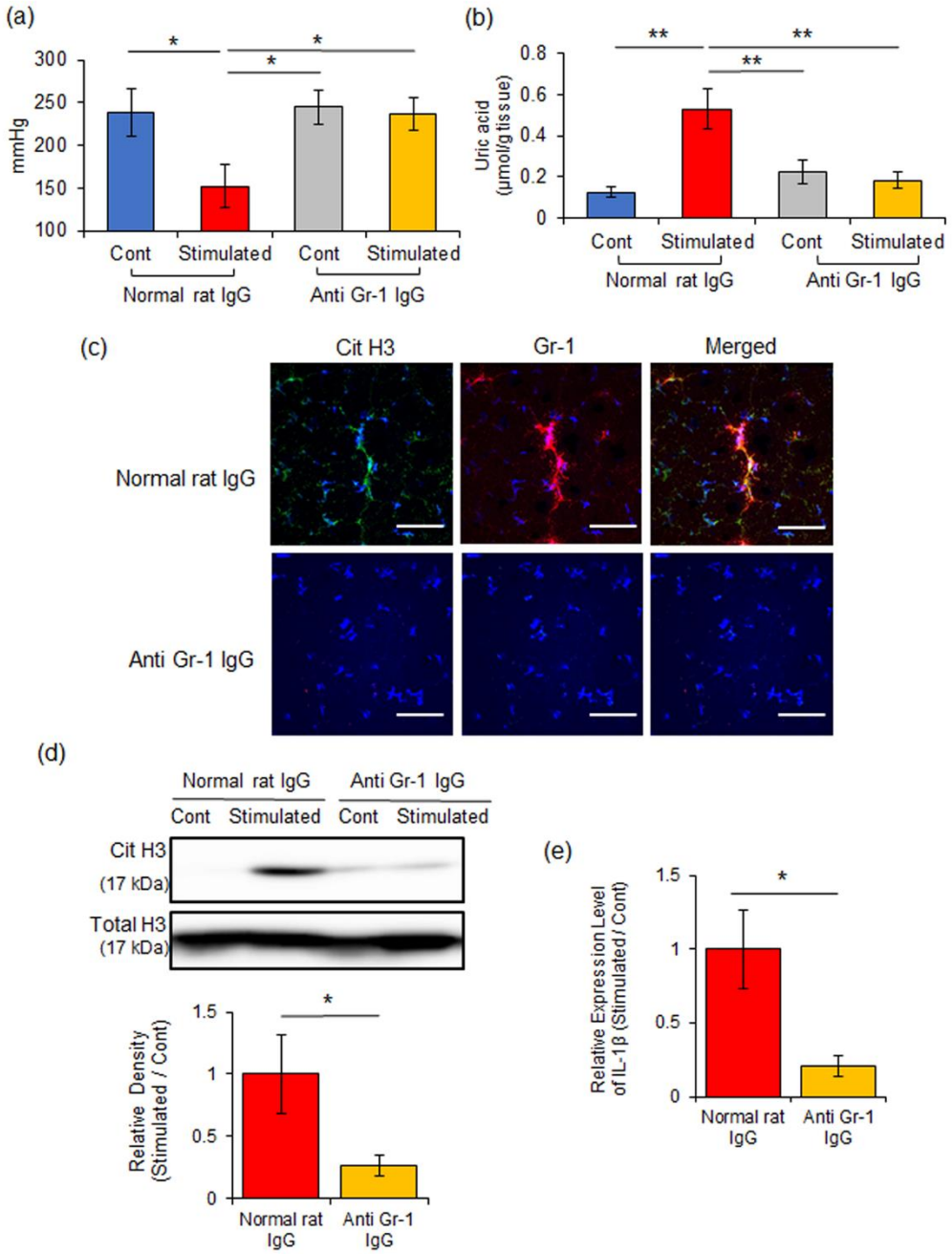
(a)
mmHg
300
250
200
150
100
Cont
Stimulated
Cont
Stimulated
Normal rat IgG
Anti Gr-1 IgG
(b)
Uric acid (μmol/g tissue)
0.8
0.6
0.4
0.2
0
Cont
Stimulated
Cont
Stimulated
Normal rat IgG
Anti Gr-1 IgG
(c)
Cit H3
Gr-1
Merged
Normal rat IgG
Anti Gr-1 IgG
(d)
Normal rat IgG
Anti Gr-1 IgG
Cont
Stimulated
Cont
Stimulated
Cit H3
(17 kDa)
Total H3
(17 kDa)
Relative Density (Stimulated / Cont)
1.5
1
0.5
0
Normal rat IgG
Anti Gr-1 IgG
(e)
Relative Expression Level of IL-1β (Stimulated / Cont)
1.5
1
0.5
0
Normal rat IgG
Anti Gr-1 IgG

Figure 5

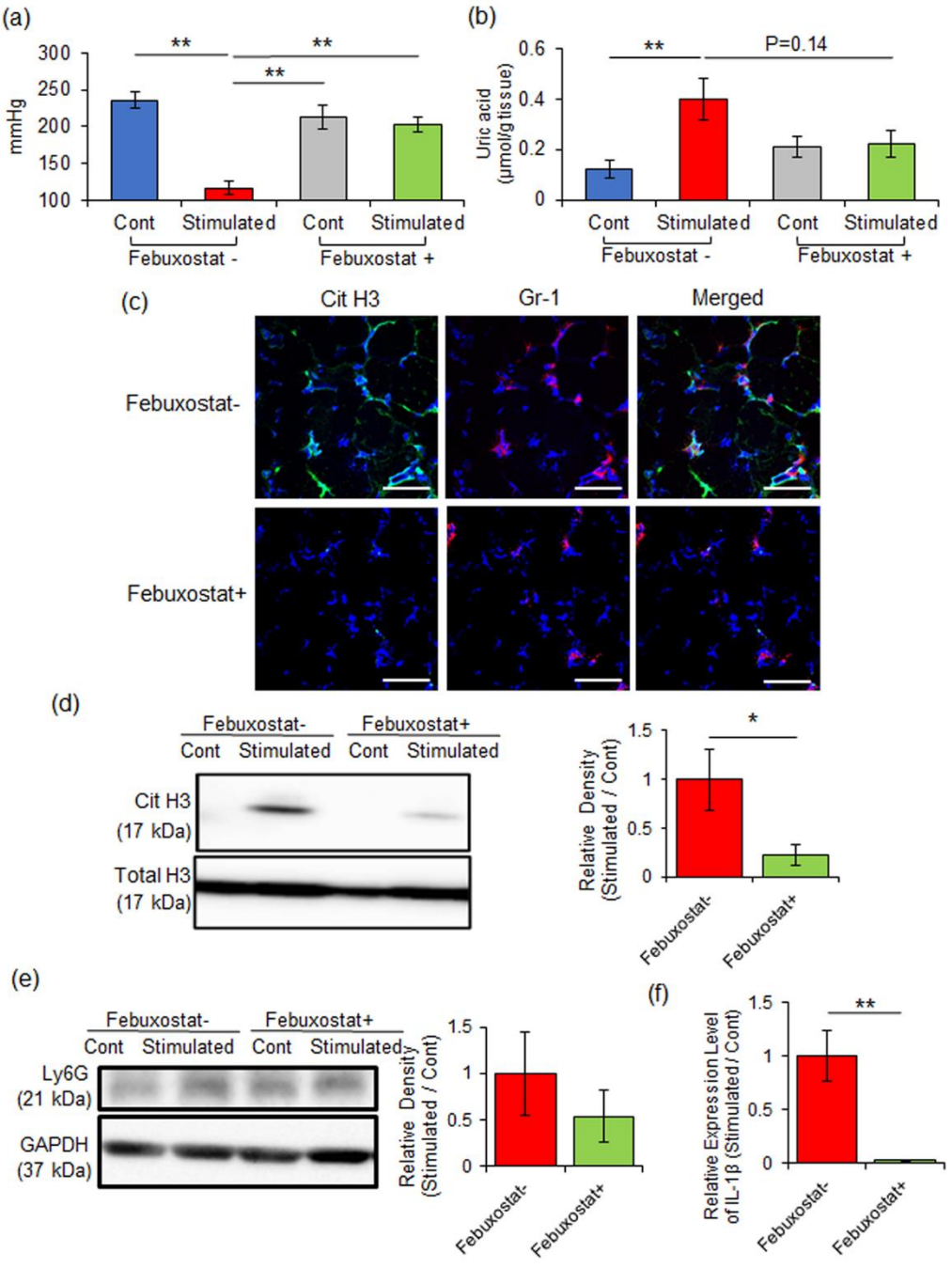
(a)
mmHg
300
250
200
150
100
**
**
**
Cont
Stimulated
Cont
Stimulated
Febuxostat -
Febuxostat +
(b)
Uric acid (μmol/g tissue)
0.6
0.4
0.2
0
**
P=0.14
Cont
Stimulated
Cont
Stimulated
Febuxostat -
Febuxostat +
(c)
Cit H3
Gr-1
Merged
Febuxostat-
Febuxostat+
(d)
Febuxostat-
Febuxostat+
Cont
Stimulated
Cont
Stimulated
Cit H3
(17 kDa)
Total H3
(17 kDa)
Relative Density
(Stimulated / Cont)
1.5
1
0.5
0
*
Febuxostat-
Febuxostat+
(e)
Febuxostat-
Febuxostat+
Cont
Stimulated
Cont
Stimulated
Ly6G
(21 kDa)
GAPDH
(37 kDa)
Relative Density
(Stimulated / Cont)
1.5
1
0.5
0
Febuxostat-
Febuxostat+
(f)
Relative Expression Level
of IL-1β (Stimulated / Cont)
1.5
1
0.5
0
**
Febuxostat-
Febuxostat+

Figure 6

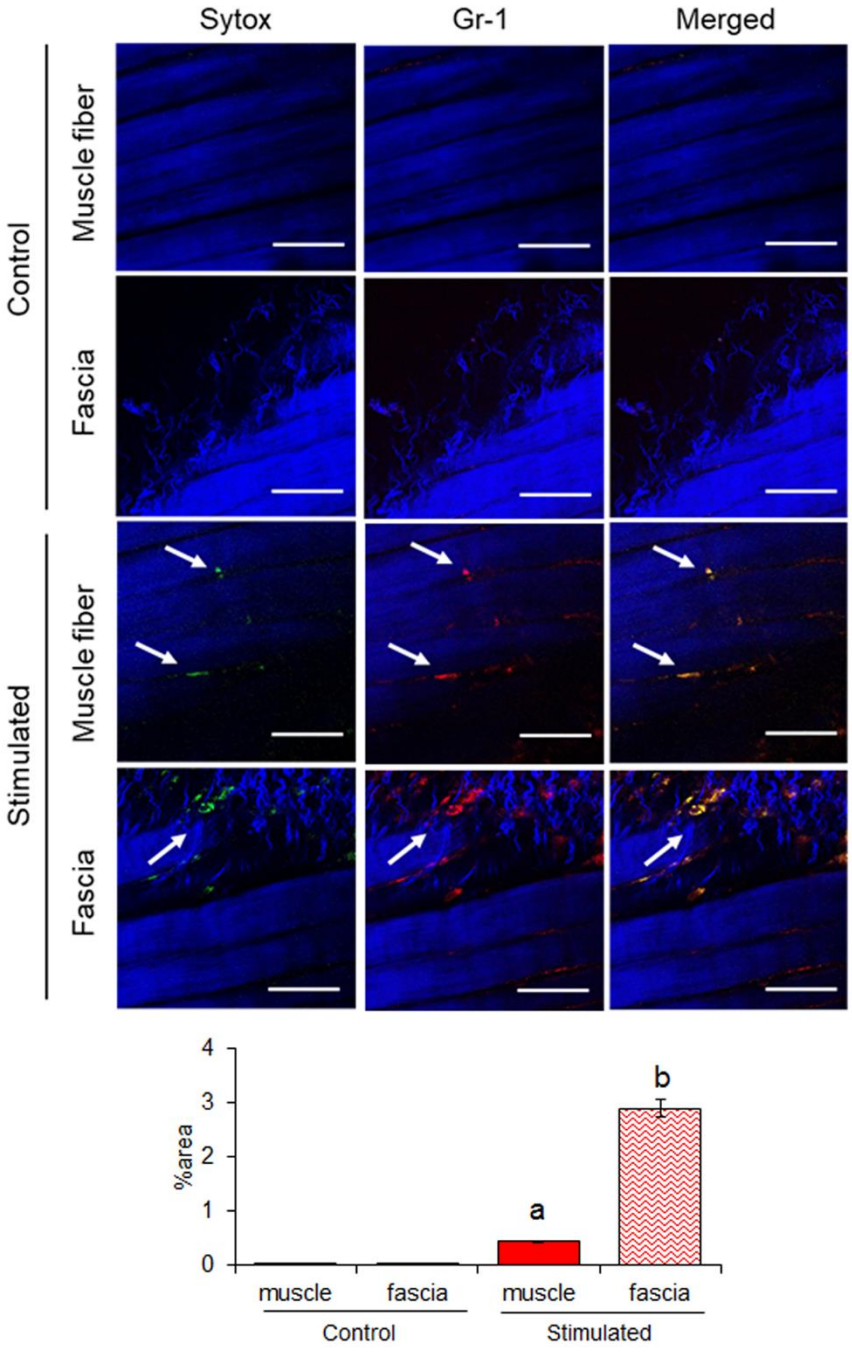
Sytox
Gr-1
Merged
Control
Muscle fiber
Fascia
Stimulated
Muscle fiber
Fascia
%area
4
3
2
1
0
a
b
muscle
fascia
muscle
fascia
Control
Stimulated

Figure 7

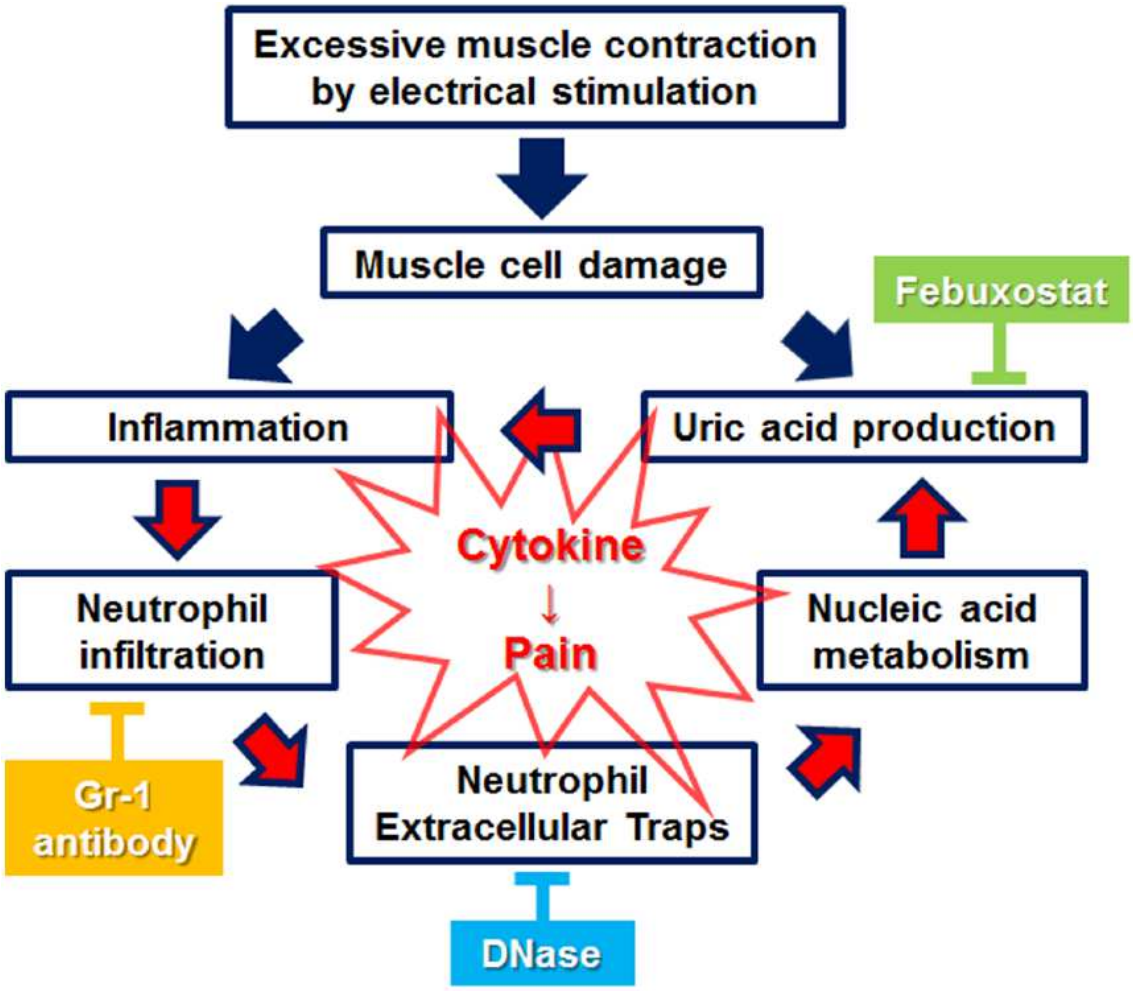
Excessive muscle contraction by electrical stimulation
Muscle cell damage
Febuxostat
Inflammation
Uric acid production
Cytokine
Pain
Neutrophil infiltration
Nucleic acid metabolism
Gr-1 antibody
Neutrophil Extracellular Traps
DNase

Supplementary Files

This is a list of supplementary files associated with this preprint. Click to download.

- Supplementalmovie1acont.mpg
- Supplementalmovie1bstimulated.mpg
- SupplementaryFigure.pdf